Electronic states in vertically ordered Ge/Si quantum dots detected by photocurrent spectroscopy

A. I. Yakimov,[1,2,*] V. V. Kirienko,[1] V. A. Armbrister,[1] A. A. Bloshkin,[1] and A. V. Dvurechenskii[1]
[1]*Rzhanov Institute of Semiconductor Physics, SB RAS, 630090 Novosibirsk, Russia*
[2]*Tomsk State University, 634050 Tomsk, Russia*
(Received 13 May 2014; revised manuscript received 16 June 2014; published 22 July 2014)

We report on intraband photocurrent spectroscopy of sixfold stacked Ge/Si quantum dots embedded in a Si matrix and aligned along the growth direction. The dots are formed in a shape of pyramids with the average lateral size of 18 nm. The *n*-type heterostructures show broad spectral response ranging from 5 to 20 μm, depending on the polarization of the incoming infrared light. The normal incidence photocurrent peak centered around 12–15 μm is attributed to the transitions from the electron states localized in the Si region adjacent to the dots to continuum states of the Si matrix. The electron confinement is caused by a modification of the conduction band alignment induced by inhomogeneous tensile strain in Si around the buried Ge/Si quantum dots. Using the Ge content and dot shape determined by Raman and scanning tunneling microscopy analysis as input parameters for three-dimensional band structure simulations, a good agreement between measured and calculated electron binding energy is obtained. Photoluminescence spectroscopy and measurements of temperature dependence of dark conductance are used to correlate photocurrent results.

DOI: 10.1103/PhysRevB.90.035430 PACS number(s): 73.21.La, 73.20.At, 71.55.Cn, 81.07.Ta

I. INTRODUCTION

In the past several years, there has been a surge of interest in nanostructures that exhibit quantum confinement in all three dimensions, which are known as quantum dots (QDs). Intersubband optical transitions in QDs have attracted a great deal of attention due to their potential applications in infrared detectors operating in mid-wave (3–4 μm) and long-wave (8–14 μm) regions where the Earth's atmosphere has its major transmission windows. Most of the demonstrations of quantum dot photodetectors were achieved with III-V self-assembled heterostructures. Ge/Si-based QD photodetectors represent another attractive type of the device due to its compatibility with the standard Si readout circuitry. At present, the most highly developed technology for fabricating arrays of Ge/Si-based QDs utilizes strain-driven epitaxy of Ge/Si nanoclusters on a Si(001) surface [1]. Ge/Si(001) QDs formed by strain epitaxy exhibit a type-II band lineup. The large ($\sim$0.7 eV) valence-band offset characteristic of this heterojunction leads to an effective localization of hole in Ge regions, which represent potential barriers for electrons. The photoresponse of *p*-type Ge/Si heterostructures with QDs in the mid-wave atmospheric window was observed by many groups [2–7] and attributed to the transitions from the hole states bound inside Ge/Si QDs to continuum states of the Si matrix.

The simple consideration of energy bands in heterostructures disregards possible modification of the band structure due to inhomogeneous strain in the dots and the surrounding matrix. In our case, the strain appears due to the $\sim$4% lattice mismatch between Si and Ge. Tensile strain in the nearby Si causes splitting of the sixfold-degenerate Δ valleys into the fourfold-degenerate in-plane Δ_{xy} valleys and the twofold-degenerate Δ_z valleys along the [001] growth direction [8–12]. The lowest conduction band edge just above and below the Ge island is formed by the Δ_z valleys yielding the triangle potential well for electrons in Si near the Si/Ge boundary. Thus one can expect three-dimensional localization of electrons in the Si region close to the apex of the Ge dots. The electron binding energy in a strain-induced potential well in an isolated Ge/Si QD was predicted to be very small ($<$10 meV) [9]. This value is expected to enlarge vastly in multilayer Ge/Si structures with vertical stacking of Ge islands due to accumulation of strain energy from different dot layers in a stack and increase of the potential well depth.

The main original point of this paper is the experimental demonstration of a zero-dimensional (0D) nature of electronic states confined near the Ge/Si quantum dots. The existence of bound electronic states produced by inhomogeneous strain distribution in a Ge/Si heterosystem has been predicted theoretically in several papers [10,11]. However, no unambiguous experimental evidence for three-dimensional electron confinement has been obtained. Neither the admittance spectroscopy in Ref. [10] nor the photoluminescence (PL) measurements in Ref. [11] can provide the information on the dimensionality of the carrier wave function. Moreover, in PL experiments, recombination of an electron with a hole occurs under conditions such that the dot is charged with the hole. Therefore one cannot discriminate between the effect of strain-induced electron localization and a confinement in a Hartree potential of positively charged QD by using PL measurements only. Although the space-charge spectroscopy [10] did give evidence for an electron accumulation in the layers of Ge/Si quantum dots containing no holes, this accumulation can be associated with a two-dimensional (2D) electron gas at the Si/Ge heterointerface and not with the 0D states. In our study, we exploit the fact that 2D quantum wells with electrons are known to be insensitive to radiation, whose polarization vector lies in the plane of the quantum well. This is because of the orthogonality of the envelopes of electron wave functions in the size quantization subbands. With respect to 2D systems, the additional in-plane confinement in a strain-induced potential well of the Si region adjacent to the dots would make the Ge/Si QDs sensitive to the normal incidence radiation. Our experiments with *n*-type layers of vertically ordered Ge/Si reveal the normal-incidence photoresponse in the spectral

*yakimov@isp.nsc.ru

range from 5 to 20 μm, thus giving evidence for the 0D nature of the confined electron states.

II. THEORETICAL CONSIDERATION

For simulation of the electronic structure for the multilayer QD stack, we considered N identical vertically aligned pyramidal Ge_cSi_{1-c} nanoclusters with four {105}-oriented facets and base orientation along [100] (x) and [010] (y) directions. The pyramids are embedded into the Si matrix and lie on the 4 ML Ge_cSi_{1-c} wetting layers. The nanoclusters are separated by Si barriers of thickness d measured from wetting layer to wetting layer. The pyramid base length l was varied from 10 nm to 30 nm in different calculations; the pyramid aspect ratio h/l is fixed and equal to 0.1. The chosen shape and size for our QDs are inspired from the experimental studies of self-assembled GeSi/Si QDs obtained in the Stranski-Krastanov growth mode [13,14] and is in agreement with the observations described in the next section. To enhance electron confinement compared to periodic GeSi/Si QD superlattices, [11] we proposed an aperiodic layer sequence. The aperiodic heterostructure consists of a thick central Si region and thin Si spacer layers surrounding it. The role of the thin Si barriers is the accumulation of elastic strain in the central part of the structure, thereby determining the depth of the potential well for electrons. The most strained thick central Si region serves for accommodation and three-dimensional confinement of electronic states. An example of such heterostructure with $N = 6$, $c = 1$, $l = 20$ nm, and $d = 5$ and 3 nm for the central Si layer and thin Si barriers, respectively, is shown in Fig. 1(a).

The finite element calculations of three-dimensional spatial distribution of strain components $\varepsilon_{\alpha\beta}$ were performed using the package COMSOL MULTIPHYSICS with the approach described in Ref. [15]. The strain tensor elements were subsequently used as input to a strain-dependent Hamiltonian. An in-plane tension and compression along the growth direction z in the Si above and below Ge islands was observed. In the lateral direction the strain in Si relaxes from the center at a scale comparable to the diameter of the underlying Ge QD and then changes its sign, demonstrating that the Si is laterally compressed around the edges of Ge islands. The final conduction band-edge alignment along the z and x directions through the center of symmetry of a sixfold stack of pure Ge islands with $l = 20$ nm is shown in Figs. 1(b) and 1(c). One can see that the potential well for electrons is more shallow in the layer plane and just its depth determines the electron binding energy E_b.

The electronic structure was calculated by solving three-dimensional effective-mass Schrödinger equation by means of a free-relaxation method. The carrier confinement potential in this equation is modified by the strain distribution. Details of theoretical consideration can be found elsewhere [10]. As expected, the electron ground state is formed by the states of two lower Δ_z valleys localized in the central Si layer close to the QD apex (red clouds in Fig. 1). Depending on the QD size, the excited electron states were found to be located either in Si spacers or in the region close to the base edges of the QDs, in agreement with the results of Refs. [11,12]. For $l = 15$–25 nm, the first excited state is a p-like state and is located also in the central Si spacer. The calculated values of the electron binding energy for the ground state E_b and the first excited state are shown in Fig. 2 for different Ge content in the dots. From the photoresponse characteristic point of view, the structures with E_b from 90 to 155 meV act as detectors with the wavelength threshold from 14 to 8 μm. Clearly, it can be seen that there is a range of reasonable dot sizes and compositions for which the photoresponse is expected in a long-wave atmospheric window.

III. SAMPLE PREPARATION AND EXPERIMENT

The Ge/Si structures were grown by solid-source molecular beam epitaxy on a p-type insulating Si(001) substrate with

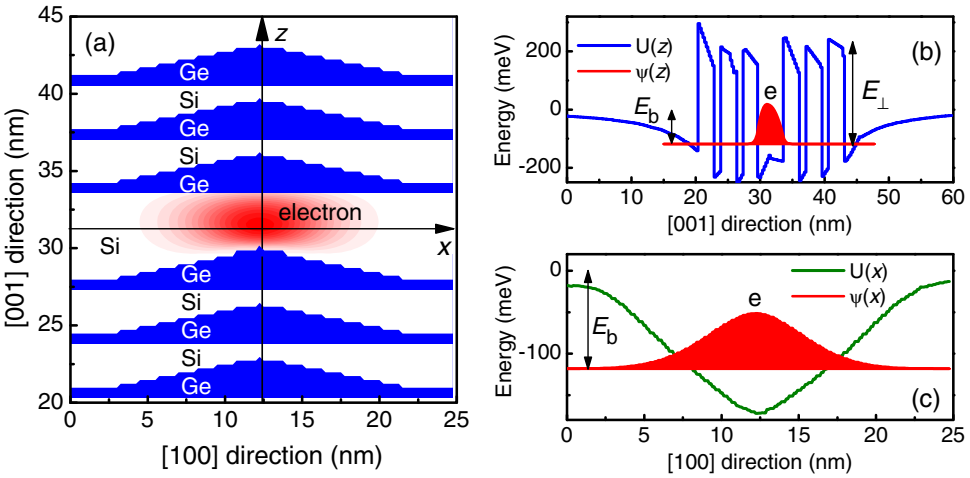

FIG. 1. (Color online) (a) Two-dimensional view of the model structure with six vertically aligned Ge QDs separated by Si. Calculated wave function of the ground electron state across the x-z plane of symmetry, cutting through the pyramids and the wetting layers, is shown in red. (b) and (c) The strain-induced confinement potential U for electrons with respect to the conduction band edge of unstrained Si along the z axis and the x axis. In a latter case the potential profile is plotted for the central Si separation layer above the tip of the Ge island. The electron wave functions ψ are shown by the red areas. The parameters of QDs are explained in the text.

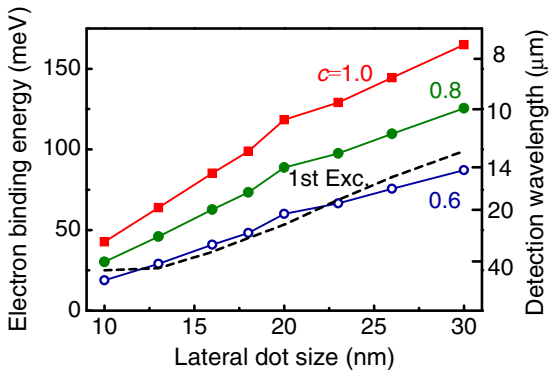

FIG. 2. (Color online) The ground-state electron binding energy E_b and respective detection wavelength λ_c in the sixfold stack of Ge_cSi_{1-c}/Si QDs as a function of pyramid base length and Ge content (c) with aspect ratio being constant. The thickness of Si layers is the same as in Fig. 1. The energy of the first excited state for $c = 0.8$ is shown by dashed line. The energy is counted with respect to the conduction band edge in unstrained bulk Si. Here we assume that λ_c relates to the binding energy as $\lambda_c(\mu\text{m}) = 1.24/E_b(\text{eV})$.

a resistivity of 150 Ω cm [Fig. 3(a)]. Samples consist of undoped Si buffer layer with 200-nm thickness, a sixfold stack of Ge/Si QDs, and a 50-nm Si cap layer. The growth temperatures were 550 and 600 °C for the cap and buffer Si layers, respectively. Ge QDs form by self-assembling in the Stranski-Krastanov growth mode at 500 °C and at a growth rate of 0.005 nm/s. The Si spacer layers were deposited at a temperature of 350 °C, with temperature ramps before

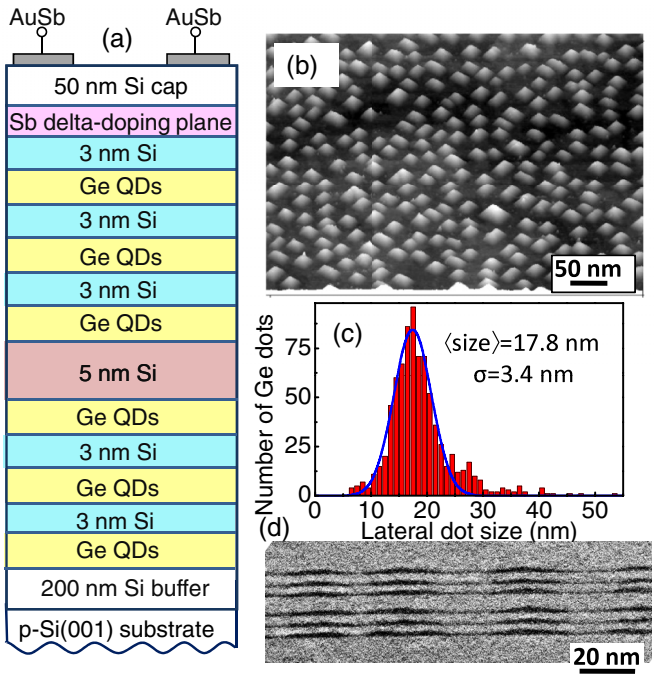

FIG. 3. (Color online) (a) Layer sequence of the Ge/Si heterostructure. (b) Three-dimensional STM image and (c) in-plane size distribution histogram from topmost uncapped Ge layer of of the Sb-doped six-layer structure. (d) Cross-sectional TEM micrograph of vertically aligned Ge QDs.

and after QD growth. This is necessary to reduce Ge-Si intermixing and to preserve the island shape and size from the effect of a further high-temperature deposition [16]. The effective thickness of the first, second, fourth, and fifth Si spacers in the stack is 3 nm, while the distance between the third and fourth Ge layers is 5 nm [Fig. 3(a)]. The n-type remote doping of the structure with Sb was achieved using an ultra-low-temperature growth technique [17–19]. A 3-nm thick undoped Si spacer was grown at 300 °C above the topmost Ge layer. The substrate temperature was then lowered at ∼3 °C/min for the Sb δ-doping layer deposition. When the substrate temperature reached 60 °C, the Sb shutter was opened to expose the sample to the Sb dose of about (3–4) × 10^{11} cm^{-2}. The Sb flux was then interrupted and the surface was covered with the 3-nm-thick Si at a rate of 0.1 nm/s [not shown in Fig. 3(a)]. After that, the substrate was reheated to 550 °C to recrystallize the layer. Epitaxial growth of the Si cap layer was then continued.

The Ge dot formation was controlled by reflection high-energy electron diffraction (RHEED) when the pattern changed from streaky to spotty. It is known that the Ge critical thickness decreases in the upper layers of a multilayer structure leading to the gradual increase of the island sizes within the island stacks from layer to layer [1,20,21]. This is due to the reduction of the strain caused by the lateral expansion of the lattice plane in the underlying island, giving rise to a reduction of the effective misfit [20]. To produce Ge islands having equal size in all layers of the sample under study the Ge growth in each layer was stopped just after the appearance of well-defined three-dimensional spots in the RHEED pattern. The final Ge coverage gradually decreased with the layer number from the bottom (0.95 nm) to the topmost Ge layer (0.8 nm). The scanning tunneling microscopy (STM) of the sample without the Si cap layer shows that Ge islands have the shape of hut clusters or pyramids bounded by {105} facets with predominantly square bases oriented along ⟨100⟩ crystallographic directions [Fig. 3(b)]. The typical base length of 18 nm and standard deviation of 3.4 nm were evaluated from the STM scans [Fig. 3(c)]. The density of the dots is about 10^{11} cm^{-2}. Cross-sectional image obtained by transmission electron microscopy (TEM) clearly shows that each Ge island in the upper layers grows on the top of the islands in the lower layers, indicating a nearly perfect vertical correlation of the dots [Fig. 3(d)]. The lateral size of QDs is nearly the same for the top and bottom layers. No misfit dislocations are observed in the sample. The average Ge content of $c = 0.83$–0.88 in the islands was determined from Raman scattering experiments using an approach described in Ref. [13].

To identify the effects of vertical dot coupling in experiments, a reference sample was fabricated under conditions similar to those described above, except that all Ge layers were separated by 10-nm-thick Si spacers. For such large dot separation, no vertical alignment of Ge islands was observed due to suppressed strain-field coupling in the thicker Si spacer.

PL measurements were carried out at $T = 78$ K using a Bruker Vertex 70 Fourier transform infrared (FTIR) spectrometer in a rapid scan mode. The FTIR system uses a calcium fluoride beamsplitter and a room temperature InGaAs detector with cutoff at 0.7 eV. The individual PL spectra were corrected with respect to the spectral sensitivity of the InGaAs detector.

PL excitation was provided by a 532-nm line of a diode yttrium aluminum garnet (YAG) laser, under an excitation power of 100 mW.

The photocurrent (PC) spectra were measured in a lateral geometry in the infrared spectral range from 50 to 300 meV. To provide ohmic contacts to the active region, AuSb strips were evaporated onto the sample surface and alloyed at 350 °C for 2 min. The distance between contacts was about 1.5 mm. The photoresponse was obtained using a FTIR system equipped with a KBr beamsplitter and a globar light source operating in a step-scan mode along with a SR570 low noise current preamplifier and a SR850 lock-in amplifier. The PC spectra were calibrated with a deuterated L-alanine doped triglycine sulfate (DLaTGS) detector. The devices were mounted in a cold finger inside a Specac cryostat with ZnSe windows.

IV. EXPERIMENTAL RESULTS AND DISCUSSION

Figure 4 depicts the comparison of PL spectra from the reference sample and the sample with vertical correlations between the QDs. The broad PL peaks from 0.7 to 0.9 eV originate from recombination of holes localized in the Ge dots and electrons confined within the tensile-strained Si around Ge islands [22–24]. The emission peak at 1.1 eV is attributed to the transverse optical (TO) phonon replica of the Si substrate [8]. The PL spectrum of the reference sample with a vertical disorder in the dot position is dominated by an emission peaked at 0.81 eV with a FWHM of ∼100 meV. The emission energy and linewidth broadening for the sample with aligned QDs are 0.75 eV and 75 meV, respectively. The integrated PL intensity is approximately the same for both structures. The reduction in the FWHM and emission energy upon dot ordering is a direct consequence of the vertical correlation and can be explained by a better size uniformity [25] and by lowering the electron energy levels in Δ_z valleys of the ordered sample. Accumulation of strain from different dot layers induces the increase of the potential well depth for electrons near the Si/Ge interface and results in a decrease of the energy of the indirect optical transition.

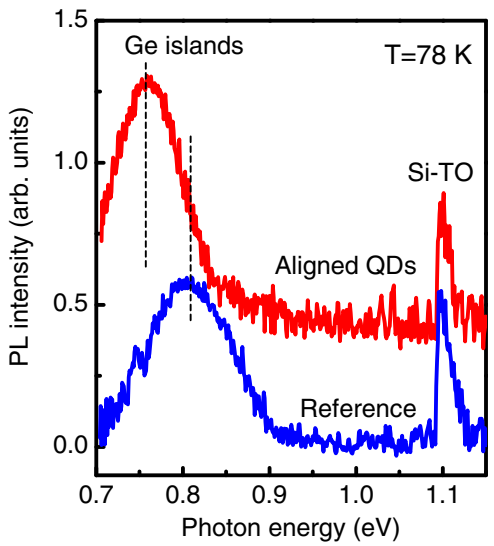

FIG. 4. (Color online) PL spectra of the reference sample and of the sample with vertical alignment of Ge QDs.

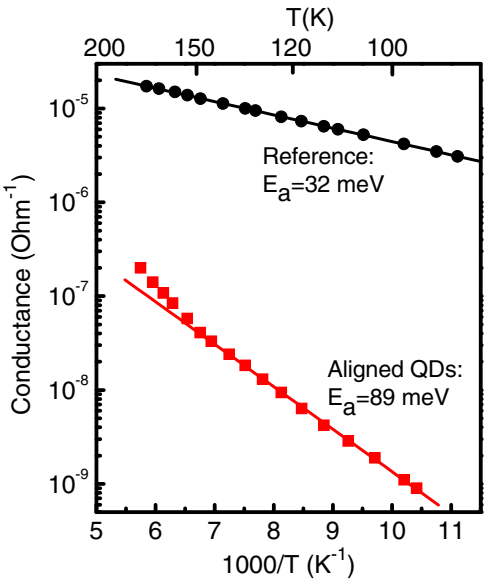

FIG. 5. (Color online) Temperature dependence of dark conductance for the reference sample and for the sample with vertical ordering of Ge QDs.

To validate the strain-related origin of the PL red shift, we measured the temperature dependence of dark conductance of the samples under investigation (Fig. 5). An Arrhenius plot of the conductance as a function of temperature yields an activation energy of $E_a = 32$ meV for the reference sample. This value is close to that reported for the ionization energy of an isolated Sb impurity state in Si ($E_i = 39$–40 meV). Therefore, the temperature dependence of conductance for the sample with no dot alignment is consistent with conduction by electrons thermally activated from the impurity states to the conduction band of the n-type Si layer. For uncoupled layers of Ge/Si dots, the electron binding energy in strain-induced potential wells is much smaller than 40 meV (Ref. [9]); the corresponding states are empty and cannot participate in charge transfer.

In the sample with closely spaced and therefore vertically ordered QDs, activated behavior is also presented but the value of the activation energy $E_a = 89$ meV is larger than that in the reference sample (Fig. 5) and close to the ground-state electron binding energy E_b calculated for the sixfold stack of Ge_cSi_{1-c}/Si QDs with $l = 18$ nm and $c = 0.8$–0.9 (Fig. 2). Because the ionization energy of the Sb impurity in Si is less than E_b, electrons leave impurities and fill deep levels in potential wells near QD apexes, resulting in a smaller conductance. Thus we can attribute the conduction mechanism in the ordered structure to the thermal excitation of electrons trapped in the Δ_z local minima of strained Si to the conduction band continuum.

Figure 6(a) shows the normal incidence photocurrent spectra of ordered QDs. The sample exhibits a PC peak centered around 80–100 meV (12–15 μm). The broad nature of the photoresponse and the asymmetric PC line shape with the flat slope on the high-energy side suggest that the photocurrent

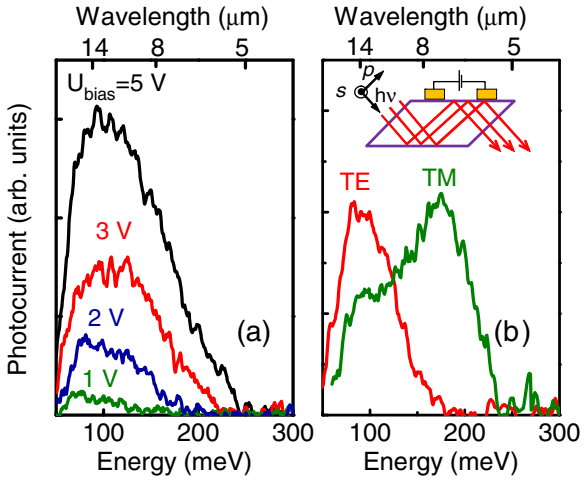

FIG. 6. (Color online) Lateral photocurrent spectra measured at $T = 85$ K (a) under normal incidence infrared radiation at various biases U_{bias} and (b) for TE and TM light polarizations at 2 V bias. Inset: the wedge coupling geometry.

could be due to a bound-to-continuum transition [4–6,26,27]. The ability of the device to operate in the normal incidence mode can be regarded as a proof of the three-dimensional confinement of electrons, unlike n-type two-dimensional systems which are not sensitive to in-plane polarized radiation [28] The observed peak position in the PC spectra excellently agrees with the measured activation energy of the dark conductance and the electron binding energy calculated for the states localized in the center of the QD stack. Since the energy separation of the ground and first excited states (∼30 meV, Fig. 2) is much larger than the thermal energy at 85 K (∼7 meV), we believe that the photocurrent originates mostly from the electron ground state. The contribution of the excited states is small and may be responsible for the low-energy tails at 50–60 meV. No response from the reference sample was detected in the spectral range of interest. Therefore, we may conclude that normal-incidence in-plane PC is caused by the optical excitation of electrons from states localized in strained Si near QD apexes to the continuum states of unstrained Si.

To test the polarization dependence of the observed PC, waveguide structures were prepared with a polished backside and polished 45° facets [Fig. 6(b)]. A KRS-5 polarizer was placed in the path of the infrared beam to select the desired beam polarization which was set either in s polarization (parallel to the dot layer plane) or p polarization (50% of the component of the electric field along the growth axis). In the geometry used, the s polarization corresponds to the transverse electric (TE) polarization. To separate transitions, which are active only for the transverse magnetic (TM) polarization (z polarization), one has to subtract 50% of the TE signal from that measured in the p polarization.

The spectra normalized to the corresponding polarized spectral intensity of the incident infrared beam are shown in Fig. 6(b). The photocurrent spectrum measured for TE polarization resembles the normal incidence photoresponse with high accuracy. In addition to the peak at ∼100 meV, the TM polarized photoresponse exhibits a strong PC peak around 200 meV. The interpretation of the 200-meV transition generated by z-polarized radiation is less obvious. We assume that it may arise due to the excitation of electrons from the same bound states in strained Si to the continuum states just above the Ge barriers, with the transition energy $E_\perp$ [see Fig. 1(b)]. The optical energy $E_\perp$ needed to overcome these barriers for heterostructure with $N = 6$, $c = 0.8$, and $l = 18$ nm is calculated to be 248 meV, which is nearly consistent with the experimental observation.

It should be noted that usually the TE-polarized absorption in conventional Stranski-Krastanov QDs is much lower than the TM-polarized response [29,30]. This is mostly due to the fact that the epitaxially grown QDs have a small height-to-base ratio (0.1 in our case), thus resembling the system with two-dimensional rather than zero-dimensional states. As a result, most of the normal incident radiation is not involved in the conversion process. For n-type Ge/Si QDs, the lateral and vertical sizes of the electron state can be comparable with each other (Fig. 1), so the dots are closer to the ideal QDs with the carrier confinement in all three dimensions. The optical activity similar in both in-plane and out-of-plane light polarization is evident in Fig. 6(b).

V. CONCLUSIONS

We have investigated the intraband photocurrent within the conduction band of GeSi/Si quantum dots. The Ge/Si islands obtained by self-organized epitaxy are vertically aligned and modulation doped with a Sb planar doping. A strong in-plane polarized photoresponse in the 8–15 μm wavelength region has been observed and ascribed to the optical excitation of electrons from states confined in the strained Si nearby the dot apexes to the continuum states of unstrained Si. Vertical ordering of the dot positions has been found to result in a decrease of the QD-related emission energy and in an increase of the activation energy of the temperature-dependent sample conductance. We have argued that all experimental observations can be reasonably explained by the formation of localized electronic states in the inhomogeneously strained Si layers. The information acquired from our study is valuable for feasible device applications.

ACKNOWLEDGMENTS

The authors are much obliged to V. A. Volodin for Raman measurements and to A. A. Shklyaev and A. K. Gutakovskii for STM and TEM experiments, respectively. This work was supported by RFBR (Grant No. 13-02-12002).

[1] K. Brunner, Rep. Prog. Phys. **65**, 27 (2002).
[2] A. I. Yakimov, A. V. Dvurechenskii, Y. Y. Proskuryakov, A. I. Nikiforov, O. P. Pchelyakov, S. A. Teys, and A. K. Gutakovskii, Appl. Phys. Lett. **75**, 1413 (1999).
[3] C. Miesner, O. Röthig, K. Brunner, and G. Abstreiter, Appl. Phys. Lett. **76**, 1027 (2000).
[4] T. Fromherz, W. Mac, A. Hesse, G. Bauer, C. Miesner, K. Brunner, and G. Abstreiter, Appl. Phys. Lett. **80**, 2093 (2002).

[5] D. Bougeard, K. Brunner, and G. Abstreiter, Physica E **16**, 609 (2003).
[6] E. Finkman, N. Shuall, A. Vardi, V. Le Thanh, and S. E. Schacham, J. Appl. Phys. **103**, 093114 (2008).
[7] A. I. Yakimov, V. A. Timifeev, A. A. Bloshkin, V. V. Kirienko, A. I. Nikiforov, and A. V. Dvurechenskii, J. Appl. Phys. **112**, 034511 (2012).
[8] O. G. Schmidt, U. Denker, K. Eberl, O. Kienzle, and F. Ernst, Appl. Phys. Lett. **77**, 2509 (2000).
[9] A. I. Yakimov, N. P. Stepina, A. V. Dvurechenskii, A. I. Nikiforov, and A. V. Nenashev, Semicond. Sci. Technol. **15**, 1125 (2000).
[10] A. I. Yakimov, A. V. Dvurechenskii, A. I. Nikiforov, A. A. Bloshkin, A. V. Nenashev, and V. A. Volodin, Phys. Rev. B **73**, 115333 (2006).
[11] D. Grützmacher, T. Fromherz, C. Dais, J. Stangl, E. Müller, Y. Ekinci, H. H. Solak, H. Sigg, R. T. Lechner, E. Wintersberger, S. Birner, V. Holý, and G. Bauer, Nano Lett. **7**, 3150 (2007).
[12] A. F. Zinovieva, A. I. Nikiforov, V. A. Timofeev, A. V. Nenashev, A. V. Dvurechenskii, and L. V. Kulik, Phys. Rev. B **88**, 235308 (2013).
[13] A. I. Yakimov, A. I. Nikiforov, A. V. Dvurechenskii, V. V. Ulyanov, V. A. Volodin, and R. Groetzschel, Nanotechnology **17**, 4743 (2006).
[14] A. I. Yakimov, G. Y. Mikhalyov, A. V. Dvurechenskii, and A. I. Nikiforov, J. Appl. Phys. **102**, 093714 (2007).
[15] M. A. S. Christiansen and H. P. Strunk, Appl. Phys. Lett. **64**, 3617 (1994).
[16] A. Rastelli, E. Müller, and H. von Känel, Appl. Phys. Lett. **80**, 1438 (2002).
[17] D. Streit, R. A. Metzger, and F. G. Allen, Appl. Phys. Lett. **44**, 234 (1984).
[18] H. P. Zeindl, T. Wegehaupt, I. Eisele, H. Oppolzer, H. Reisinger, G. Templel, and F. Koch, Appl. Phys. Lett. **50**, 1164 (1987).
[19] J. Blacksberg, M. E. Hoenk, and S. Nikzad, J. Crystal Growth **285**, 473 (2005).
[20] J. Tersoff, C. Teichert, and M. G. Lagally, Phys. Rev. Lett. **76**, 1675 (1996).
[21] V. Le Thanh, V. Yam, P. Boucaud, Y. Zheng, and D. Bouchier, Thin Solid Films **369**, 43 (2000).
[22] H. Sunamura, N. Usami, Y. Shiraki, and S. Fukatsu, Appl. Phys. Lett. **66**, 3024 (1995).
[23] M. W. Dashiell, U. Denker, C. Müller, G. Costantini, C. Manzano, K. Kern, and O. G. Schmidt, Appl. Phys. Lett. **80**, 1279 (2002).
[24] U. Denker, M. Stoffel, O. G. Schmidt, and H. Sigg, Appl. Phys. Lett. **82**, 454 (2003).
[25] W.-H. Chang, W.-Y. Chen, A.-T. Chou, T.-M. Hsu, P.-S. Chen, Z. Pei, and L.-S. Lai, J. Appl. Phys. **93**, 4999 (2003).
[26] D. Pan, E. Towe, and S. Kennerly, Appl. Phys. Lett. **73**, 1937 (1998).
[27] A. D. Stiff, S. Krishna, P. Bhattacharya, and S. Kennerly, Appl. Phys. Lett. **79**, 421 (2001).
[28] B. Levine, J. Appl. Phys. **74**, R1 (1993).
[29] J. Shao, T. E. Vandervelde, A. Barve, A. Stintz, and S. Krishna, Appl. Phys. Lett. **101**, 241114 (2012).
[30] V. Y. Panevin, A. N. Safronov, L. E. Vorobjev, D. A. Firsov, V. A. Shalygin, M. Y. V. ans R. M. Balagula, A. A. Tonkikh, P. Werner, B. Fuhrman, and G. Schmidt, Semiconductors **47**, 1574 (2013).